Asia-Pacific Journal of Atmospheric Sciences (2020) 56:45–56
https://doi.org/10.1007/s13143-019-00129-6

Online ISSN 1976-7951
Print ISSN 1976-7633

ORIGINAL ARTICLE

The Impact of a New Set of IASI Channels on the Unified Model Global Precipitation Forecast

Young-Chan Noh[1,2] · Byung-Ju Sohn[1] · Yoonjae Kim[3]

Received: 9 January 2019 / Revised: 17 April 2019 / Accepted: 30 April 2019 / Published online: 10 May 2019

Abstract

This study attempts to assess the impact of data assimilation with newly selected Infrared Atmospheric Sounding Interferometer (IASI) channels on the global precipitation forecast, using the Korea Meteorological Administration (KMA) Unified Model (UM) system. The new IASI channels assimilated under the clear-sky condition give a positive impact on the global precipitation forecast, shown in the trial experiments. In particular, the overestimated horizontal size of forecasted precipitation in the control run with operational IASI channels significantly decreases in the experimental trial with the newly selected channels. In addition, the moist biases of moisture field in the model analysis as an initial condition are substantially reduced in the experiment run. Considering that the moisture in the troposphere is a main source of precipitation, the reduction of moist biases in the troposphere seems to contribute to the improvement of precipitation forecast in the UM system. Therefore, these results suggest that the improved moisture field even over clear areas is able to enhance the precipitation forecast accuracy. And because the difference between two trial runs is only a set of IASI channels used in the UM data assimilation system, the improved precipitation forecast is likely to due to the use of different H_2O channels in the new set of IASI channel used in the experiment run, which are sensitive to the tropospheric water vapor.

Keywords Data assimilation · Precipitation · Hyper-spectral sounder · Unified model

1 Introduction

Precipitation is one of most important weather forecasting parameters, because it can affect our daily living. In particular, accurate forecasting of heavy rainfall and flood is much valuable to the public; earlier preparation can reduce potential damages caused by heavy rain events. In recent years, with advances in the numerical modeling skills and significant increase of used observations for the initialization of the NWP model, forecast accuracies including precipitation forecast have been significantly improved (English et al. 2000; Simmons and Hollingsworth 2002; Dee et al. 2011; Bauer et al. 2015). Along with the current horizontal and vertical finer resolution of NWP models, increased computational power was thought to be technical advances essential for the improved forecasting accuracy. Such development and efforts now allow us to include more detailed representation of precipitation-associated dynamical and thermodynamic processes in the NWP model (Shapiro et al. 2010; Kumar et al. 2016; Wang et al. 2016).

Despite the continuous progress in forecasting performance, precipitation is still thought to be the most difficult variable to predict. One main reason is because parameterizations described in model physics are over-simplified, not realistically reflecting the non-linear relationship between cloud/precipitation processes and model state variables (Ebert et al. 2007; Zhang et al. 2013). Aiming at the better description of such non-linear relationship, most studies have focused on improving the parameterizations of cloud and precipitation physics (Hong 2004; Hong et al. 2004; Thompson et al. 2004, 2008; Morrison et al. 2009; Lim and Hong 2010; Liu et al. 2011).

Responsible Editor: Lei Bi.

✉ Young-Chan Noh
ynoh3@wisc.edu

[1] School of Earth and Environmental Sciences, Seoul National University, Seoul, South Korea

[2] Cooperative Institute for Meteorological Satellite Studies, University of Wisconsin–Madison, 1225 West Dayton St., Madison, WI 53706, USA

[3] National Institute of Meteorological Sciences, Korea Meteorological Administration, Jeju, South Korea

Besides improved parameterization, accurate initial condition is also considered to be an important factor for better precipitation forecasting since the weather prediction is fundamentally an initial value problem (Lorenc 1986; Kalnay 2003). From the assimilation of precipitation-affected microwave radiances in the WRF model, Zhang et al. (2013) showed a positive impact on the heavy rain event over the United States. Updated hydrometeors from microwave radiance assimilation were considered to be the cause of such positive impact on the heavy rain event. More recently, Han et al. (2016) attempted to assimilate the microwave radiances in the forecasting of Hurricane Sandy (2012) and Typhoon Haiyan (2013) cases. In their study, only the cloud-screened microwave radiances were used for the data assimilation in the WRF model, and thus the hydrometeors were not directly updated during the assimilation process, but rather environment field around a typhoon was updated. Nevertheless, the accuracy of TC forecasts was improved, suggesting that improved surrounding environmental field can also enhance the forecasting accuracy of severe weather phenomena in the NWP model forecasts. In particular, Han et al. study is meaningful since the typhoon forecasting was improved through improved environmental fields over the clear-sky area (by better removing cloud-contaminated microwave scenes) near the typhoon rain bands. The surrounding environments such as wind and moisture fields should be more realistic for predicting the typhoon better in the model.

Recently, Noh et al. (2017) suggested a new set of IASI channels for the UM data assimilation. In trial experiments, it was shown that environmental fields such as upper tropospheric humidity in the NWP model can be improved with the new channel set of data, compared to the channel set operationally used in the UM data assimilation system. Thus, with the consideration of the fact that better environmental condition is able to improve the typhoon forecast in the model as suggested by Han et al. (2016), precipitation forecast may be also improved with the new selection of IASI channels by improving moisture field in the precipitation environment, which is a main source of precipitation formation.

In this study, we attempt to examine how the improved moisture field gives rise to the precipitation forecasting through the trial experiments using the operational UM system at the KMA. While all the observations are kept same in the operational UM data assimilation system except IASI observations from two set of IASI channels – operationally used 183 channels vs. 200 channels from Noh et al. (2017). Impact assessment will be made by comparing the trial results from two different set of IASI channels. Obtained results will shed light on how the improved environment gives influences on the precipitation forecasting and/or on how the new set of IASI channels give rise in the improved precipitation forecasting.

The paper is organized as follows. Section 2 provides a summary of data used in this study. And the characteristics of new IASI channels are presented in section 3 where the data assimilation system for numerical experiment is also described. In section 4, the impact of newly selected IASI channels on the UM global precipitation forecast is presented, followed by summary and conclusions in section 5.

2 Used Data

2.1 IASI Observations

IASI instrument is onboard the EUMETSAT MetOp satellites, which measures the emitted radiances in 8461 channels over the infrared spectrum range of 645–2760 cm^{-1} at a spectral resolution of 0.5 cm^{-1} (Siméoni et al. 1997). Providing precise vertical information on the temperature and water vapor due to the high spectral resolution and low radiometric noise, IASI observations have been actively assimilated to enhance the forecasting accuracy at NWP centers (Collard and McNally 2009; Hilton et al. 2009; Guidard et al. 2011; Hilton et al. 2012).

However, because of operational limitations associated with data assimilation system (e.g., high data volume, heavy computational cost, and the capability of its NWP system), different subsets of channels among whole IASI channels are used for the assimilation at the NWP centers. In the UM system at the KMA (as well as at the UK Met Office), 183 channels among originally distributed 314 EUMETSAT channels have been used for the assimilation (Collard 2007; Weston 2011). In recent study, new 200 channels among 314 channels were suggested to maximize the use of atmospheric information from the IASI observations in the assimilation process (Noh et al. 2017). Compared with 183 channels used for the operational forecasting, 149 channels among operational 183 channels are also included in the new IASI 200 channels and 51 channels are only shown in the new channel set. Fifty-one channels are mainly distributed over the O_3 (1030 cm^{-1}), H_2O (1350–2000 cm^{-1}) absorption bands and in band 3 (2000–2760 cm^{-1}) (Fig. 1). In the shortwave infrared IASI band 3, H_2O (2000–2050 cm^{-1}) and CO_2 (4.3 μm) absorption bands are also located. Details about the channel selection and impact of new channels on the humidity field are found in Noh et al. (2017).

2.2 Precipitation Data for Validation

Precipitation forecasting results are validated against independent satellite-based observation data. To assess the global precipitation forecasting from trial experiments, we use

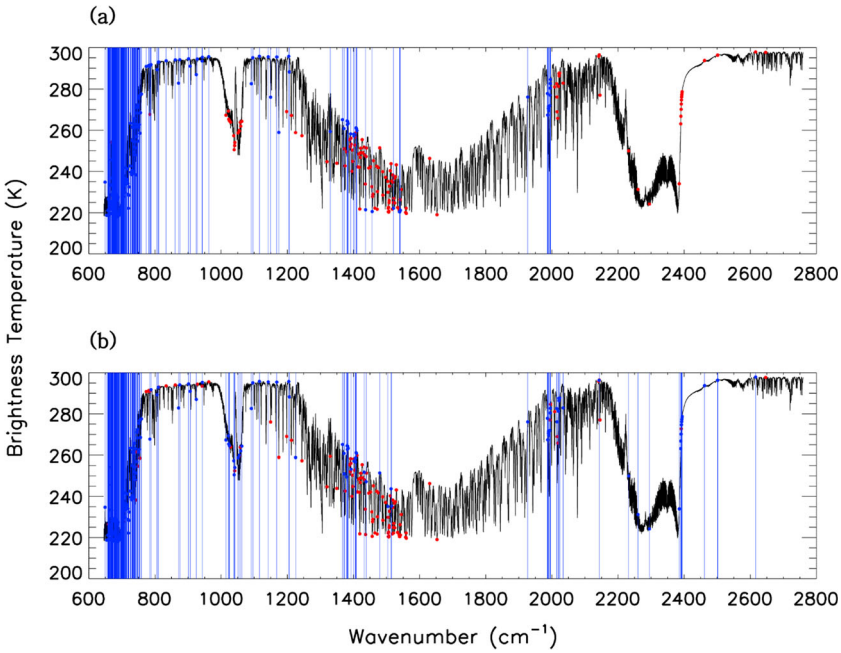

Fig. 1 Spectral distribution (black line) of (**a**) the operational 183 IASI channels and **b** the newly selected 200 channels over the infrared spectral band (600–2800 cm^{-1}). Blue bars and red dots indicate the selected IASI channels and remaining channels among the provisional 314 IASI channels, respectively

precipitation products of IMERG (Hou at al. 2014; Draper et al. 2015; Skofronick-Jackson et al. 2017). The IMERG algorithm intends to integrate various precipitation data from microwave-based precipitation measurements, microwave-calibrated infrared estimates, and surface gauge observations. IMERG is designed to compensate limited samples from single LEO satellite, with all available LEO satellites. Temporal and spatial gaps in the IMERG microwave precipitation estimate are filled by GEO-infrared satellite measurements using a morphing technique (Liu 2016; Asong et al. 2017; Huffman et al. 2017). IMERG products are half-hourly with a spatial resolution of 0.1° × 0.1°.

2.3 Total Precipitable Water

In order to evaluate the TPW of UM analysis, satellite-based TPW data are used as a reference, which are obtained from the MiRS (Boukabara et al. 2010, 2011, 2013). The system employs microwave measurements from the AMSU and MHS sensors onboard NOAA-18, NOAA-19, MetOp-A, and MetOp-B platform, and the SSMIS from DMSP-F16 and DMSP-F18 platform. In this study, we only use the TPW data over the ocean. Because of the sampling times of polar-orbiting satellites for MiRS TPW, data are selected for the comparison if satellite overpass time is within 30 min from the model analysis time (i.e., 00000 UTC and 1200 UTC). Data were downloaded from NOAA Comprehensive Large Array-Data Stewardship System (https://www.class.ncdc.noaa.gov).

3 Data Assimilation System and Experiment Design

In order to examine the impact of the new set of IASI channels on the UM global precipitation forecasts, global assimilation trials are conducted for a period from 15 June to 31 July 2015, using the global data assimilation system at the KMA. The analysis period has been chosen because the Northern Hemisphere summer period should have various global precipitation events. The spatial resolution of the UM system used for the trial experiment is N320 L70 (about 40 km in mid-latitudes) with 70 vertical levels from the surface to 80 km. The model used for data assimilation has a horizontal resolution of N216 L70 (about 60 km) with 70 vertical levels. Used assimilation scheme is a 4D-Var scheme, having the assimilation time window from −3 to +3 h centered at the nominal T + 0 analysis time.

In this study, we used the bias correction scheme embedded in the UM data assimilation system, which was suggested by Harris and Kelly (2001) for satellite measurements. In this correction scheme, the geometric thicknesses of the 850–300 hPa, and 200–50 hPa pressure layers from the model output are used as predictors, which regress to the first-guess departures between satellite-observed radiances and modelled radiances. In the case of IASI measurements, pre-calculated bias correction coefficients for each of IASI 314 channels are used to predict the biases for selected IASI channels assimilated. Since this study aims to examine the impact of newly selected IASI channels on the global precipitation forecast, same bias corrections coefficients were employed for two trial runs.

Before assimilating the IASI data, a quality control process known as the OPS embedded in the UM system is performed. Once the IASI measurements are compared with the forward-modelled radiances from model atmospheric fields (called the background) using a RTM. In the UM, the 6-h forecasts derived from the previous data assimilation cycle are employed as a background. And then, by examining the departure between the satellite-observed radiances and model-simulated radiances, a quality of both satellite measurements and model background is monitored. In addition to the examination of departure, a 1D-Var is carried out to examine that the IASI data are adequate for the UM 4D-Var data assimilation system. If the 1D-Var minimization is failed, the IASI data are not assimilated (Hilton et al. 2009).

The trials are comprised of control and experiment runs. Operational 183 IASI channels are used for the control run. In the experiment run, those operational IASI channel data are substituted with the new 200 IASI channel data suggested by Noh et al. (2017). But O_3 channels are removed from 200 IASI channels in the experiment run because of the same reason for the operational system that ozone vertical profiles are not specifically predicted in the UM model and instead are replaced by its climatological values. In addition, shortwave infrared channels in the IASI band 3 are used during the night time only (solar zenith angle >95°) because of solar contamination during the daytime. Overall the experiment run uses 189 channels amongst the new set of 200 IASI channels during the nighttime but only 163 channels during the daytime. Apart from different IASI channels, all the same baseline observations including ground-based and satellite observations are used for both trial runs, which are listed in Table 1.

Table 1 Observation types assimilated in the UMl used in this study. See the Appendix for explanation of acronyms

Observation type	Platform
AMDAR	Aircraft
AIREP	Aircraft
PILOT	Sonde
Dropsonde	Sonde
Wind profiler	Sonde
SYNOP	Land surface
BUOY	Sea surface
SHIP	Sea surface
AIRS radiances	Aqua
AMSU-A/MHS radiances	MetOp series, and NOAA series
AMVs (GEO)	MSG series, GOES series, MTSAT, and COMS
AMVs: MODIS	Aqua and Terra
ATMS radiances	S-NPP
CrIS radiances	S-NPP
GEO radiances	MSG series and COMS
GPSRO bending angle	COSMIC, MetOp series/GRAS, and GRACE
HIRS radiances	NOAA series
IASI radiances	MetOp series
Microwave imager sea surface wind	Coriolis/Windsat
Scatterometer sea surface wind	MetOp series/ASCAT
SSMIS radiances	DMSP series

4 Results

4.1 Assessment of Precipitation Forecast

To stabilize the model initial condition generated throughout the data assimilation process for the trial runs, sixteen days (i.e., 15 June – 30 June 2015) were allowed for the spin-up. Thus, accuracy of global precipitation forecast was evaluated for two trial runs for a period from 1 July 2015 to 31 July 2015, using the TS and BS, defined in Eqs. (1) and (2) respectively, as an evaluation index.

$$\text{Threat Score (TS)} = \frac{Hits}{Hits + Misses + False\ Alarms} \quad (1)$$

$$\text{Bias Score (BS)} = \frac{Hits + False\ Alarms}{Hits + Misses} \quad (2)$$

"*Hits*" represents the intersection area of precipitation between model forecast and reference data, "*Misses*" is the precipitation area in the reference data but missed by the model forecast. "*False Alarms*" indicates the precipitation area in the forecast, but not assigned as the precipitation area in reference data. Thus, TS has a value between 0 and 1, and higher (lower) value represents better (poorer) forecast performance for each trial run. The BS is the ratio of horizontal extent of precipitation area in the forecast to the reference data, implying whether the forecast system has a tendency to underestimate (BS < 1) or overestimate (BS > 1) the precipitation area in the model forecast (Wilks 1995; Ahijevych et al. 2009).

For the calculation of TS and BS, either satellite-based IMERG precipitation data or precipitation field from model analysis can be used as a reference. Considering that the UM 4D-Var data assimilation system comprises an update cycle with the assimilation time window from −3 to +3 h centered at the T + 0 analysis time, the T + 0 analysis data are normally considered as initial conditions, which are used as a reference in this study. After the end of the data assimilation process at each cycle, the hydrometeors related to the cloud/precipitation are generated by the dynamical and thermodynamic system embedded in the UM system, which is run from T-3 h to the analysis time at T + 0 h (Field et al. 2011). Therefore, the precipitation products at the analysis time can be used as a reference, with the purpose of assessing the forecasted

precipitation. Precipitation rate is in mm h^{-1} and a threshold of 0.1 mm h^{-1} is used for discriminating "precipitation" from "no precipitation". In this study, the analysis domain is limited within the 60°N–60S° as shown in Fig. 2, because IMERG-produced global precipitation covers the 60°N–60S° domain. As shown in Fig. 2, large amount of precipitation is intensively distributed over the ITCZ and East Asian monsoon regions during the summer season of 2015.

Forecasts are first validated against observation data (observation verification) and results are shown in Fig. 3. Results show that mean TS at T + 0 forecast hour is about 0.27 for both control and experiment runs, and it decreases with longer forecast time; for example, the TS values decrease around 0.22 at T + 48 forecast hour. The decreasing tendency with forecast hour suggests that the precipitation forecast deteriorates with forecasting hour. Furthermore, TS values generally smaller than 0.3 over all forecasting hours indicate that the model forecasts are in lack of predicting exact locations of precipitation area, against observations.

Validation is also made against the model analysis (analysis verification) for the same mean TS value, and results show that TS magnitudes are substantially larger than against satellite observations. It is likely because of the fact that analysis at each trial run is employed for evaluating its own forecast field. It is noted that both runs (control and experiment run) show little difference in TS, meaning that use of new set of IASI channels for the data assimilation gives little improvement in terms of the precipitation location.

Mean biases of two experiments against observation and model analysis are calculated and mean BS values at forecast hours between T + 0 and T + 48 for the control and the experiment runs are shown in Fig. 4. The mean BS values against observations for two trial runs are about 1.5 at T + 0 forecast hour and these values increase with forecast hours; for example, values are slightly larger than 1.6 at T + 48 h. The values larger than 1.5 indicate that the UM model tends to overestimate the total precipitation area by 150% to 160%, in comparison to the satellite-based precipitation area.

But it is noted that the mean BS values for the experiment run are smaller than for the control run by about 1%–3%, suggesting that the new set of IASI channels improves the precipitation forecast in term of precipitation horizontal area. In contrast, comparison against model analysis shows that the mean BS values for the experiment run are slightly larger than for the control run. It seems to be due to more overestimated precipitation area in the analysis for the control, as shown in the BS values against observations at T + 0 forecast hour.

We also examine forecast accuracy depending on the precipitation intensity, by dividing the precipitation intensity in six ranges of 0.1–0.5, 0.5–1.0, 1.0–5.0, 5.0–10.0, 10.0–20.0 and > 20 mm h^{-1}. Bias scores at these six ranges are given in Fig. 5. With interest, the bias score is largely separated into two types; BS for precipitation rate < 5 mm h^{-1} vs. BS for precipitation rate > 5 mm h^{-1}. Such BS difference suggests that the UM model tends to overestimate the precipitation area for the light precipitation cases (< 5.0 mm h^{-1}) while underestimate the area for medium to heavy precipitation (> 5.0 mm h^{-1}). One might think that it is associated with the spatial resolution of the model used in this study (about 40 km). It is because more intense precipitation often occurs

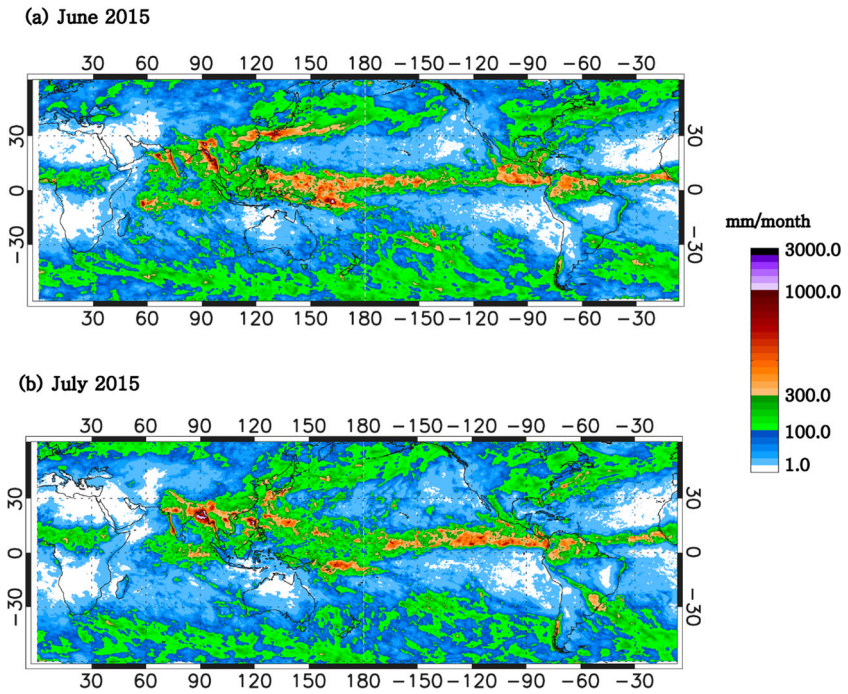

Fig. 2 Spatial distribution of monthly-accumulated precipitation (mm $month^{-1}$) for (**a**) June 2015 and **b** July 2015 using IMERG products

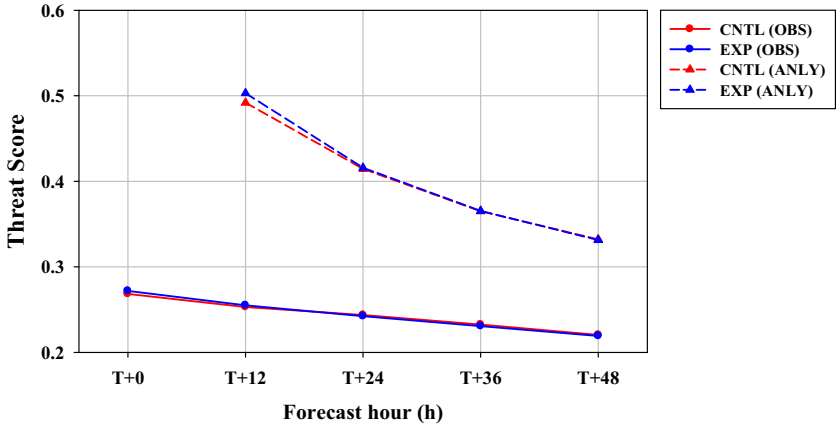

Fig. 3 TSs of global precipitation forecast for the UM at the KMA for a period from 1 July −31 July 2015. Red and blue lines indicate the control and experiment runs, respectively. Solid and dashed lines represent the validation results using the observation and analysis data produced at each trial run, as a reference

in an organized fashion such as in a form precipitation band, and thus high-resolution model may be necessary to resolve the heavy precipitation event. However, considering the finding that even higher resolution UM models (i.e., N512 L70 (about 25 km) and N768 L70 (about 17 km)) also show the similar contrast (Oh et al. 2015), the current result suggests that the UM model tends to overpredict the light precipitation area while underpredict the heavier precipitation area.

Since the total precipitation area is largely modulated by the area showing the light precipitation, the overall overestimate of the total precipitation area described in Fig. 4 is likely due to the overestimated light precipitation area. In addition, the increasing trend of BS values with forecast hour is also shown in the light precipitation area, not heavy precipitation area. Thus, the better accuracy of precipitation area for the experiment run (in Fig. 4) is likely due to the improved light precipitation area especially weaker than 5 mm h^{-1} (shown in Fig. 5). Because the difference between two trial runs using the UM data assimilation system is a set of IASI channels used in their data assimilation process, the reduction of overestimated light precipitation area can be attributed to new selected IASI channels used in the experiment run.

4.2 Assessment of Environmental Moisture Field

As noted in Han et al. (2016) of the hurricane forecasting, the improved surrounding environmental field can enhance the accuracy of the precipitation forecast. In this context, we assume that the improved precipitation forecast shown in Fig. 4 may be attributed to the improved environmental field. Considering that there is no difference of model physics of cloud and precipitation for two trial runs and the hydrometeors in the model are not directly updated in the assimilation process, this assumption is believed to be reasonable. Here we expect improved moisture field because the more accurate moisture distributions are at least necessary condition for the better precipitation forecast, and assess how moisture fields might be improved from the use of new set of IASI channels.

In order to assess the change in moisture field from the use of new IASI channels, mean differences in relative humidity and mixing ratio profiles of analysis field between two trial runs (experiment run minus control run) are compared, which were obtained by taking average of 1 July to 31 July 2015 (Fig. 6). In Fig. 6, it is shown that the initial condition for the experiment run is drier over the nearly entire troposphere except 500 hPa – 600 hPa levels, compared to for the control

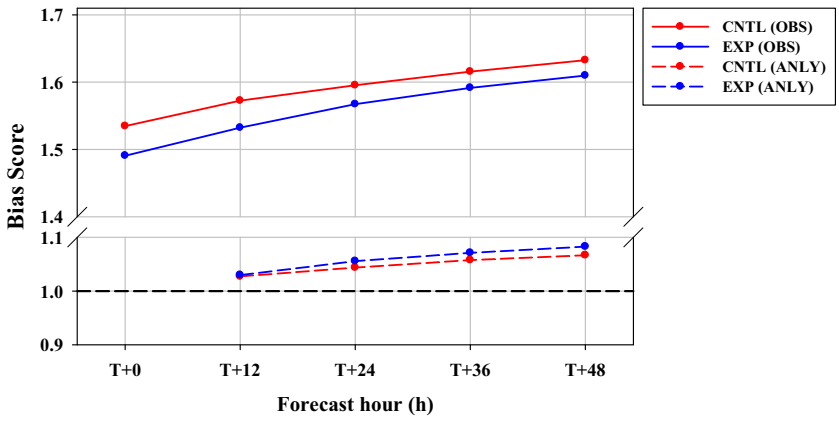

Fig. 4 BSs of global precipitation forecast for the UM at the KMA for a period from 1 July −31 July 2015, using the observation data as a reference. Red and blue lines indicate the control and experiment runs, respectively. Solid and dashed lines represent the validation results using the observation and analysis data produced at each trial run, as a reference

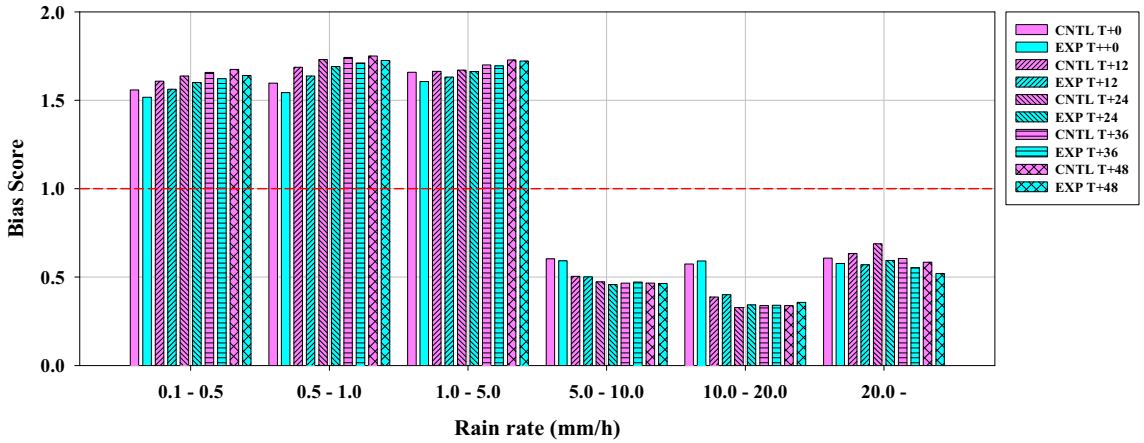

Fig. 5 Histogram of BSs of global precipitation forecast depending on the rain rate for a period from 1 July −31 July 2015. Pink and cyan indicate the control and the experiment runs, respectively. Various texture patterns in the vertical bars represent the forecast hours for both the control and the experiment runs

run. Even though large difference in relative humidity appears in the upper troposphere (100 hPa – 500 hPa) rather than in the lower troposphere (600 hPa – 1000 hPa), the difference in mixing ratio is larger in the lower layers. However, this comparison results only indicate that the moisture field of initial state for the experiment run is relatively dryer than for the control run. Thus, we made an attempt to validate the moisture field of initial condition for two trial runs using independent satellite-based moisture products.

In order to evaluate the moisture field of the model initial condition (analysis), the satellite-based TPW data as a reference are used. The collocated data were made by matching MiRS retrieved TPW data within the collocation time window from −30 to +30 min centered at the UM model analysis time (i.e., 0000 UTC and 1200 UTC) over the region within the 60°N–60S°. The time series of the mean TPW bias for two trial runs against the satellite-based TPW are shown in Fig. 7. Positive biases are consistently found at both trial runs for a period from 1 July to 31 July 2015, but the bias for the experiment run is significantly reduced by an average of 38% as compared to for the control run. The reduction of TPW bias is mainly induced by the decrease of moisture content in the lower troposphere below 650 hPa level for the experiment run, as shown in Fig. 6b. Consequently, considering that the precipitation is a product of the condensation of water vapor in the air, the decreased moisture content of initial condition for the experiment run seems to lead to the reduction of light precipitation area (< 5.0 mm h^{-1}) in the model forecast. The improved moisture field of initial condition is mainly attributed to the additional H_2O channels in the IASI band 3 (2000–2760 cm^{-1}) used during the night time only, which are not in the operational 183 channels - see Fig. 4 of Noh et al. (2017). In particular, the H_2O channels over 2000–2050 cm^{-1} absorption band have low weighting function peak in the troposphere, providing additional water vapor information in the lower troposphere where most moisture content exists.

However, considering that the operational 183 channels also include the low-tropospheric H_2O channels, it is not logical to claim that the improved model moisture is simply due to the added low-tropospheric H_2O channels. Thus, we further examined the bias correction process in which the observed radiances are corrected. As a result, it is found that the low-tropospheric H_2O channels in the new channel set have different bias correction coefficients compared with the H_2O channels in the operational channel set. As explained in Section 3, the statistic bias correction suggested by Harris and Kelly (2001) is used as a bias correction scheme in the UM, which is employed to remove the bias errors including the instrument errors and uncertain radiative transfer modelling. A linear bias predictor model is defined in Eq. (3).

$$b = \beta_0 + \sum_{i=1}^{N} \beta_i p_i \tag{3}$$

where β_0 indicates the constant component of bias b and β_i are the bias correction coefficients of the predictors p_i associated with the channels. The subscript i denotes the number of predictors (i.e., $i = 1,2\ldots N$). In the UM, the geometric thicknesses of the 850–300 hPa and 200–50 hPa are used as predictors. The correction coefficients (β_i) and constant component (β_0) are predefined by regressing the first-guess departure to the model predictors. In this scheme, it is assumed that the model background (i.e., 6-h forecast) is unbiased, meaning that the most of biases originate from the observation error and systematic errors (e.g., uncertainty of radiative transfer modeling). However, the background field from current model can be biased, so the model bias can be also merged in the constant component (β_0) in a form of satellite radiance in the process of

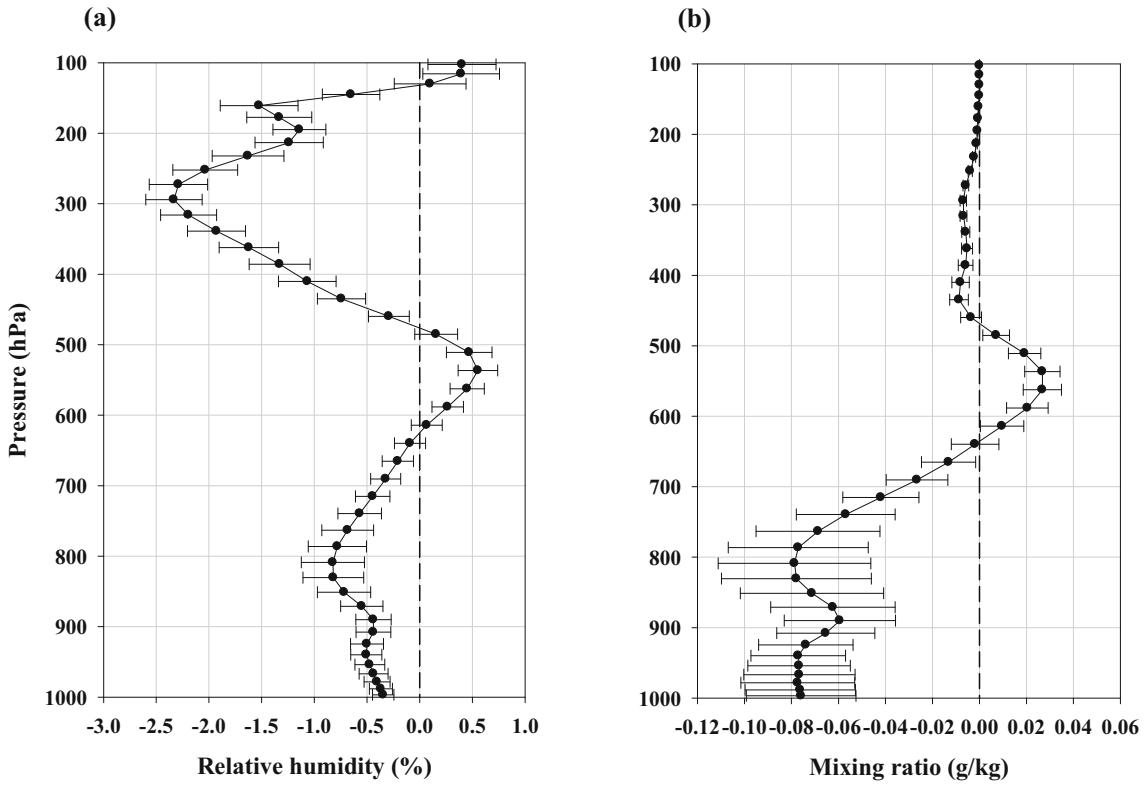

Fig. 6 Mean difference of (**a**) relative humidity (%) and **b** mixing ratio (g kg^{-1}) for analysis between control run and experiment run for a period from 1 July −31 July 2015. Horizontal bars representing one standard deviation are overlaid

computing the bias correction coefficients. In practice, it is quite difficult to separate the contribution of model bias from the estimated biases. But, because the IASI sensor is known as a well-calibrated sensor and the performance of radiative transfer modeling has significantly improved, the bias pattern of model background can be diagnosed from the pre-defined β_0.

Considering that the model background has a humid bias in the troposphere, as shown for the TPW validation (Fig. 7), it is expected that the β_0 for lower-tropospheric H_2O channels have positive values, because the simulated background radiances tend to decrease with the moisture amount in the troposphere. These positive β_0 are shown for most lower-tropospheric H_2O channels except three channels (Fig. 8).

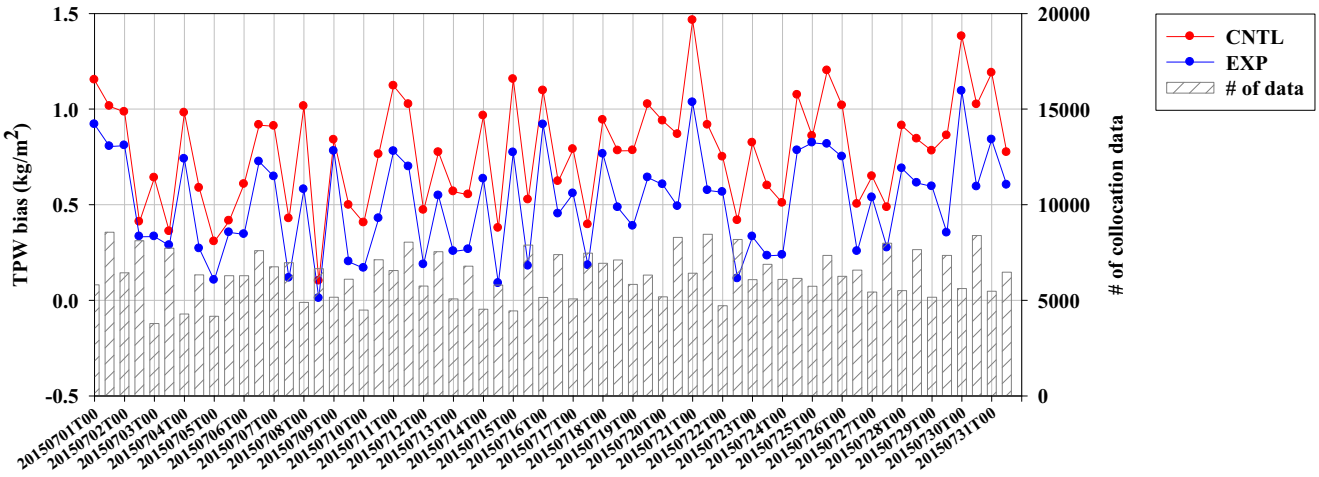

Fig. 7 Time series of mean TPW biases between model forecasts and satellite-retrieved data for a period from 1 July −31 July 2015. Red and blue lines indicate the control and experiment runs. Vertical bars represent the number of collocated data between model forecast and observation data

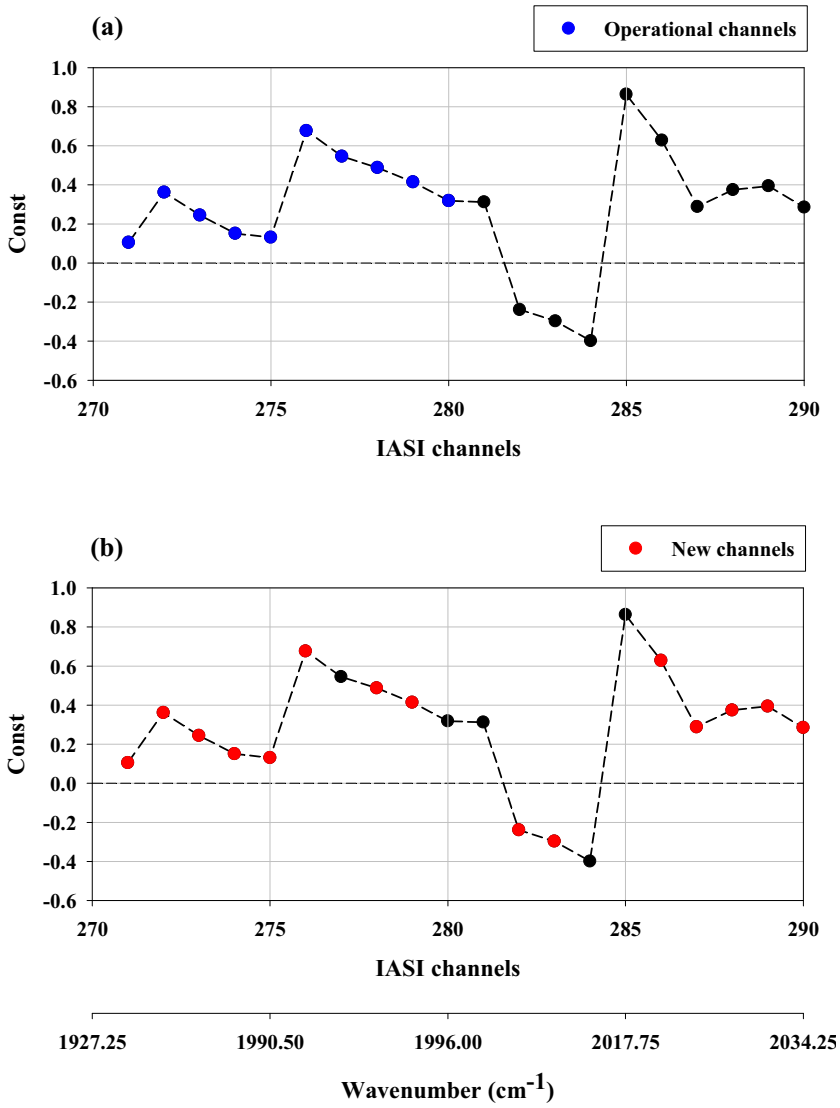

Fig. 8 The constant component of bias (β_0) for IASI H_2O channels. Blue and red circles indicate the operational H_2O channels and the newly selected channels, respectively

Using the operational channels, the humid bias of model background could not be corrected by the assimilating the lower troposphere H_2O channels, as the signal of model humid bias is eliminated by the bias correction process using positive β_0 (Fig. 8a). However, as shown in Fig. 8b, two of newly selected H_2O channels (corresponding to channel wave numbers 2014.75 and 2015.50 cm^{-1}) have negative β_0 values, which result from the combination of biases from unknown sources. Consequently, assimilating two H_2O channels with different bias correction coefficients seems to contribute to reducing the humid bias of model moisture, compared with using the operational channels.

It is also interesting to note that, although the TPW bias for the experiment run is smaller than for the control run, the initial conditions for two trial runs still have humid biases (up to 1.5 kg m^{-2}). The bias pattern of moisture field might be attributed to the model spatial resolution used in this study (about 40 km) because simulated moisture processes (e.g., evaporation, convection, precipitation, and cloud) in the model significantly vary depending on the model resolution (Sperber et al. 1994; Phillips et al. 1995; Hertwig et al. 2014; Rashid and Hirst 2016). Thus, to investigate the resolution-dependency of moisture bias, the moisture field of initial condition from the operationally used global UM system with a high spatial resolution of N768 L70 (about 17 km) is validated against the MiRS TPW data for a one-year period (1 July 2016 – 30 June 2017) (Fig. 9). Similar to the results shown in Fig. 7, the operational UM model tends to overestimate the moisture field with a humid bias by a maximum of about 2.0 kg m^{-2} for a summer period (July – August 2016). In addition, it is noted that weak humid biases are still shown in other seasons except summer season, suggesting that the global UM system tends to overestimate the moisture field overall regardless of the model horizontal resolution.

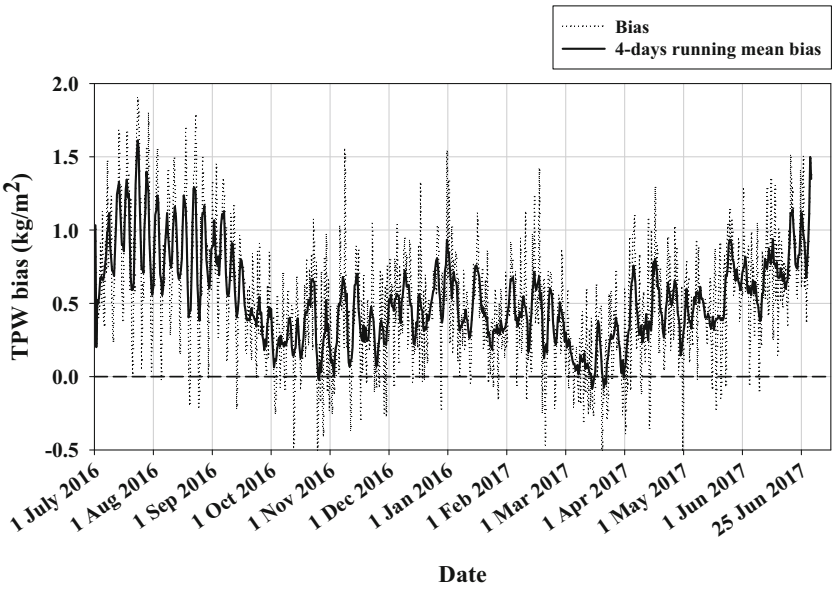

Fig. 9 Time series of mean TPW biases between operational UM (N768 L70) analysis at the KMA and satellite-retrieved TPW products for a period from 1 July 2016 – 30 June 2017. Solid and dashed lines indicate the four-days-running-mean bias and the daily mean bias, respectively

In summary, humid bias of moisture field in the model is significantly reduced by assimilating new selected IASI channels, leading to the reduction of the overpredicted precipitation area in the model forecast. Considering that a set of IASI channels used in the data assimilation system are only difference between two trial runs, the improved precipitation forecast seems to be attributed to the use of different H_2O channels in the new set of channels, which are sensitive to the water vapor in the troposphere.

5 Summary and Conclusions

In a recent study, Noh et al. (2017) introduces a new set of IASI channels assimilated in the UM system, which significantly reduces large positive humidity bias in the troposphere shown in the operational UM forecast with the operational IASI channels. With the consideration of the fact that moisture in the air becomes water droplets and ice crystals, leading to the formation of cloud and precipitation, the improved moisture field with new channels might also contribute to enhancing the precipitation forecast in the model. Thus, in this study, we further attempt to assess the impact of a new set of IASI channels on the precipitation forecast in the UM global model, compared to the operationally used channels. Two trial experiments are conducted for a summer period from 15 June to 31 July 2015, using the global UM data assimilation system at the KMA. Operational 183 IASI channels are assimilated in the control run. In the experiment run, these IASI channels are substituted with newly selected IASI channels suggested by Noh et al. (2017). Except for the IASI observations, same baseline observations are used for two trial runs.

The TS values, as an indicator in terms of precipitation location accuracy, are little different between two trial runs and decrease with forecast hours for both runs. For the BS results, two trial runs have large positive biases increasing with forecast hours, which are evidently shown in the light precipitation area (< 5.0 mm h^{-1}). However, positive biases of BS significantly decrease in the experiment run, in particular, in the light precipitation area, meaning that the overestimated precipitation area in the model forecast is reduced by assimilating new IASI channels in the UM system.

In the validation of moisture content in the model initial condition, it is found that large humid bias is shown in the control run but for the experiment run the positive bias significantly decreases. Thus, based on the fact that the precipitation is a product originating from the atmospheric moisture, the reduction of overestimated precipitation area in the model forecast area seems to be attributed to the improved moisture field in the model initial condition. Furthermore, because the difference between two trial runs is only a set of IASI channels assimilated in the UM system, the improved precipitation forecast seems to be due to additional H_2O channels in the newly selected channels, conveying the moisture information in the troposphere. In particular, two channels of added low-tropospheric H_2O channels have different bias coefficients compared with operational H_2O channels, mainly leading to the reduction of model humid bias in the troposphere.

Acknowledgements This research was supported by the Korea Meteorological Administration Research and Development Program under Grant KMIPA KMI2018-06910, and was also supported by the BK21 Plus Project of the Korean government.

APPENDIX

Glossary of Terminology and Abbreviations

1D-Var	One-dimensional variational data assimilation
4D-Var	Four-dimensional variational data assimilation
AIREP	Aircraft report
AIRS	Atmospheric Infrared Sounder
AMDAR	Aircraft Meteorological Data Relay
AMSU-A	Advanced Microwave Sounding Unit-A
AMV	Atmospheric motion vector
Aqua	Satellite in EOS series
ASCAT	Advanced Scatterometer
BS	Bias Score
COMS	Communication, Ocean and Meteorological Satellite
COSMIC	Constellation Observing System for Meteorology Ionosphere and Climate
DMSP	Defense Meteorological Satellite Program
EUMETSAT	European Organization for the Exploitation of Meteorological Satellites
GEO	Geosynchronous orbiting (satellite)
GOES	Geostationary Operational Environmental Satellite
GPM	Global Precipitation Measurement
GPSRO	Global Positioning System Radio Occultation
GRAS	GNSS Receiver for Atmospheric Sounding
HIRS	High Resolution Infrared Radiation Sounder
IASI	Infrared Atmospheric Sounding Interferometer
IMERG	Integrated Multi-satellite Retrievals for GPM
ITCZ	Intertropical Convergence Zone
KMA	Korea Meteorological Administration
LEO	Low-Earth orbiting (satellite)
MetOp	Meteorological Operational satellite series operated by EUMETSAT
MHS	Microwave Humidity Sounder
MiRS	Microwave Integrated Retrieval System
MODIS	Moderate Resolution Imaging Spectroradiometer
MSG	Meteosat Second Generation
MTSAT	Multifunctional Transport Satellite
NOAA	National Oceanic and Atmospheric Administration
NWP	Numerical Weather Prediction
OPS	Observation Processing System
PILOT	Upper-level wind observation
RTM	Radiative Transfer Model
SHIP	Sea surface weather observation by ship
S-NPP	Suomi National Polar-orbiting Partnership
SSMIS	Special Sensor Microwave Imager/Sounder
SYNOP	Land surface synoptic weather observation
TC	Tropical cyclone
TS	Threat Score
Terra	Satellite in EOS series
TPW	Total Precipitable Water
UM	Unified Model
WindSat	Polarimetric microwave radiometer on Coriolis
WRF	Weather Research and Forecast

References

Ahijevych, D., Gilleland, E., Brown, B., Ebert, E.: Application of spatial forecast verification methods to gridded precipitation forecasts. Weather Forecast. **24**, 1485–1497 (2009)

Asong, Z.E., Razavi, S., Wheater, H.S., Wong, J.S.: Evaluation of integrated multisatellite retrievals for GPM (IMERG) over southern Canada against ground precipitation observations: a preliminary assessment. J. Hydrometeorol. **18**, 1033–1050 (2017)

Bauer, P., Thorpe, A., Brunet, G.: The quiet revolution of numerical weather prediction. Nature. **525**, 47–55 (2015)

Boukabara, S.-A., Coauthors: A physical approach for a simultaneous retrieval of sounding, surface, hydrometeor, and cryospheric parameters from SNPP/ATMS. J. Geophys. Res. Atmos. **118**, 12600–12619 (2013)

Boukabara, S.-A., Garrett, K., Chen, W.: Global coverage of total precipitable water using a microwave variational algorithm. IEEE Trans. Geosci. Remote Sens. **48**, 3608–3621 (2010)

Boukabara, S.-A., Garrett, K., Chen, W., Iturbide-Sanchez, F., Grassotti, C., Kongoli, C., Chen, R., Liu, Q., Yan, B., Weng, F., Ferraro, R., Kleespies, T., Meng, K.: MiRS: an all-weather 1DVAR satellite data assimilation and retrieval system. IEEE Trans. Geosci. Remote Sens. **49**, 3249–3272 (2011)

Collard, A.D.: Selection of IASI channels for use in numerical weather prediction. Q. J. R. Meteorol. Soc. **133**, 1977–1991 (2007)

Collard, A.D., McNally, A.P.: The assimilation of infrared atmospheric sounding interferometer radiances at ECMWF. Q. J. R. Meteorol. Soc. **135**, 1044–1058 (2009)

Dee, D.P., Coauthors: The ERA-interim reanalysis: configuration and performance of the data assimilation system. Q. J. R. Meteorol. Soc. **137**, 553–597 (2011)

Draper, D.W., Newell, D.A., Wentz, F.J., Krimchansky, S., Skofronick-Jackson, G.M.: The global precipitation measurement (GPM) microwave imager (GMI): instrument overview and early on-orbit performance. IEEE J. Sel. Topics Appl. Earth Obs. Remote Sens. **8**, 3452–3462 (2015)

Ebert, E.E., Janowiak, J.E., Kidd, C.: Comparison of near-real-time precipitation estimates from satellite observations and numerical models. Bull. Am. Meteorol. Soc. **88**, 47–64 (2007)

English, S.J., Renshaw, R.J., Dibben, P.C., Smith, A.J., Rayer, P.J., Poulsen, C., Saunders, F.W., Eyre, J.R.: A comparison of the impact of TOVS and ATOVS satellite sounding data on the accuracy of numerical weather forecasts. Q. J. R. Meteorol. Soc. **126**, 2911–2931 (2000)

Field, P.R., Bodas-Salcedo, A., Brooks, M.E.: Using model analysis and satellite data to assess cloud and precipitation in midlatitude cyclones. Q. J. R. Meteorol. Soc. **137**, 1501–1515 (2011)

Guidard, V., Fourrié, N., Brousseau, P., Rabier, F.: Impact of IASI assimilation at global and convective scales and challenges for the assimilation of cloudy scenes. Q. J. R. Meteorol. Soc. **137**, 1975–1987 (2011)

Han, H., Li, J., Goldberg, M., Wang, P., Li, J., Li, Z., Sohn, B.J., Li, J.: Microwave sounder cloud detection using a collocated high resolution imager and its impact on radiance assimilation in tropical cyclone forecasts. Mon. Weather Rev. **144**, 3937–3959 (2016)

Harris, B.A., Kelly, G.: A satellite radiance bias correction for data assimilation. Q. J. R. Meteorol. Soc. **127**, 1453–1468 (2001)

Hertwig, E., von Storch, J.S., Handorf, D., Dethloff, K., Fast, I., Krismer, T.: Effect of horizontal resolution on ECHAM6-AMIP performance. Clim. Dyn. **45**, 185–211 (2014)

Hilton, F., Coauthors: Hyperspectral earth observations from IASI: five years of accomplishments. Bull. Amer. Meteorol. Soc. **93**, 347–370 (2012)

Hilton, F., Atkinson, N.C., English, S.J., Eyre, J.R.: Assimilation of IASI at the met Office and assessment of its impact through observing system experiments. Q. J. R. Meteorol. Soc. **135**, 495–505 (2009)

Hong, S.-Y.: Comparison of heavy rainfall mechanisms in Korea and the Central United States. J. Meteorol. Soc. Japan. **82**, 1469–1479 (2004)

Hong, S.-Y., Dudhia, J., Chen, S.-H.: A revised approach to ice microphysical processes for the bulk parameterization of clouds and precipitation. Mon. Weather Rev. **132**, 103–120 (2004)

Hou, A., Coauthors: The global precipitation measurement Mission. Bull. Am. Meteorol. Soc. **95**, 701–722 (2014)

Huffman, G.J., Bolvin, D.T., Braithwaite, D., Hsu, K., Joyce, R., Kidd, C., Nelkin, E.J., Sorooshian, S., Tan, J., Xie, P.: NASA global precipitation measurement (GPM) integrated multi-satellite retrievals for GPM (IMERG). Algorithm theoretical basis document (ATBD), Version 5.1, NASA, 34 pp (2017)

Kalnay, E.: Atmospheric modeling, data assimilation, and predictability. Cambridge University Press (2003)

Kumar, P., Ojha, S.P., Singh, R., Kishtawal, C.M., Pal, P.K.: Performance of weather research and forecasting model with variable horizontal resolution. Theor. Appl. Climatol. **122**, 1–9 (2016)

Lim, K.-S.S., Hong, S.-Y.: Development of an effective double-moment cloud microphysics scheme with prognostic cloud condensation nuclei (CCN) for weather and climate models. Mon. Weather Rev. **138**, 1587–1612 (2010)

Liu, Z.: Comparison of integrated multisatellite retrievals for GPM (IMERG) and TRMM multisatellite precipitation analysis (TMPA) monthly precipitation products: initial results. J. Hydrometeorol. **17**, 777–790 (2016)

Liu, C., Ikeda, K., Thompson, G., Rasmussen, R., Dudhia, J.: High-resolution simulations of wintertime precipitation in the Colorado headwaters region: sensitivity to physics parameterizations. Mon. Weather Rev. **139**, 3533–3553 (2011)

Lorenc, A.C.: Analysis methods for numerical weather prediction. Q. J. R. Meteorol. Soc. **112**, 1177–1194 (1986)

Morrison, H., Thompson, G., Tatarskii, V.: Impact of cloud microphysics on the development of trailing stratiform precipitation in a simulated squall line: comparison of one- and two-moment schemes. Mon. Weather Rev. **137**, 991–1007 (2009)

Noh, Y.-C., Sohn, B.-J., Kim, Y., Joo, S., Bell, W., Saunders, R.: A new infrared atmospheric sounding interferometer channel selection and assessment of its impact on Met Office NWP forecasts. Adv. Atmos. Sci. **34**, 1265–1281 (2017). https://doi.org/10.1007/s00376-017-6299-8

Oh, J., Ryu, G.-H., Kim, Y., Kim, D.-J.: Evaluation of global precipitation forecast using the satellite-based precipitation estimates of TMPA and GPM. NIMR-TN-2015-004, p75 (in Korean) (2015)

Phillips, T.J., Corsetti, L.C., Grotch, S.L.: The impact of horizontal resolution on moist processes in the ECMWF model. Clim. Dyn. **11**, 85–102 (1995)

Rashid, H.A., Hirst, A.C.: Mechanisms of improved rainfall simulation over the maritime continent due to increased horizontal resolution in an AGCM. Clim. Dyn. **49**, 1747–1764 (2016)

Shapiro, M., Coauthors: An earth-system prediction initiative for the twenty-first century. Bull. Am. Meteorol. Soc. **91**, 1377–1388 (2010)

Siméoni, D., Singer, C., Chalon, G.: Infrared atmospheric sounding interferometer. Acta Astronautica. **40**, 113–118 (1997)

Simmons, A.J., Hollingsworth, A.: Some aspects of the improvement in skill of numerical weather prediction. Q. J. R. Meteorol. Soc. **128**, 647–677 (2002)

Skofronick-Jackson, G., Coauthors: The global precipitation measurement (GPM) mission for science and society. Bull. Am. Meteorol. Soc. **98**, 1679–1695 (2017)

Sperber, K.R., Hameed, S., Potter, G.L., Boyle, J.S.: Simulation of the northern summer monsoon in the ECMWF model: sensitivity to horizontal resolution. Mon. Weather Rev. **122**, 2461–2481 (1994)

Thompson, G., Rasmussen, R.M., Manning, K.: Explicit forecasts of winter precipitation using an improved bulk microphysics scheme. Part I: description and sensitivity analysis. Mon. Weather Rev. **132**, 519–542 (2004)

Thompson, G., Field, P.R., Rasmussen, R.M., Hall, W.D.: Explicit forecasts of winter precipitation using an improved bulk microphysics scheme. Part II: implementation of a new snow parameterization. Mon. Weather Rev. **136**, 5095–5115 (2008)

Wang, X., Steinle, P., Seed, A., Xiao, Y.: The sensitivity of heavy precipitation to horizontal resolution, domain size, and rain rate assimilation: case studies with a convection-permitting model. Adv. Meteorol. **2016**, 1–20 (2016)

Weston, P.: Progress towards the implementation of correlated observation errors in 4D-Var. Forecasting Research Tech. Rep. 560, Met Office, Exeter, UK (2011)

Wilks, D.S.: Statistical methods in atmospheric science. Academic Press, New York (1995)

Zhang, S., Zupanski, M., Hou, A., Lin, X., Cheung, S.: Assimilation of precipitation-affected radiances in cloud-resol ving WRF ensemble data assimilation system. Mon. Weather Rev. **141**, 754–772 (2013)